Monostatic RCS Prediction from Irregularly Distributed Near-Field Samples Using Plane-Wave Field Synthesis

Ole Neitz[1], Thomas F. Eibert[1]
[1]Chair of High-Frequency Engineering, Department of Electrical and Computer Engineering
Technical University of Munich (TUM), Munich, Germany, ole.neitz@tum.de

***Abstract*—We present an approach to accurately determine the monostatic RCS of an object under test, by measuring a set of bistatic near-field scattering data, where it is sufficient to sample the scattered field in a small angular range around the transmitting antenna. This is achieved by solving a field synthesis problem for the incident plane wave with respect to the transmitter locations and using the result to weight the outcome of a series of inverse source problems. By expanding the fields in propagating plane waves on the unit sphere, almost arbitrary scan surfaces can be processed efficiently, including highly irregular ones. Thus, the measurement samples of the scattered field may potentially be collected by the use of unmanned aerial vehicles and it may even become possible to determine the RCS of large stationary outdoor targets. The paper outlines the theory of the algorithm and demonstrates its capabilities by means of simulated and measured near-field data.**

***Index Terms*— near-field measurements, unmanned aerial vehicle (UAV), radar cross section (RCS) measurement, plane-wave field synthesis.**

I. Introduction

To accurately measure the radar cross section (RCS) of an arbitrary object under test, far-field (FF) or compact-range facilities are typically employed to realize a plane-wave illumination of the object [1], [2]. In the latter case, this is achieved by large reflectors, synthesizing the field of a plane wave within a specified area, called the quiet zone. In order to avoid the large spatial requirements and high costs of these facilities, there is an ongoing interest in applying near-field (NF) measurement techniques, mostly developed for antenna measurements, also for determining the RCS [3]–[5]. It is well known that with a full set of bistatic NF measurements the RCS may be perfectly recovered [6]. However, as acquiring such a set is unfeasible in most cases, the main challenge is to work with only a limited set of bistatic data or only monostatic NF data, which motivated the development of RCS extrapolation and prediction techniques [5], [7]–[9]. Most of these methods are based on the linearized model of independent scattering centers and are therefore said to be image-based [5]. While accurate results can still be achieved for many scenarios, these approaches usually perform poorer if strong multiple interactions occur, as it is the case for more complex shaped targets [10]. Using a set of bistatic NF data this problem may be overcome, as it was shown for a 2D cylindrical setup in, e.g., [11], where it was also demonstrated that only a limited angular range of samples on a circular arc may be sufficient. However, in order to employ an efficient cylindrical modal expansion of the fields, the approach is limited to acquiring the measurement samples on circles (or spheres in the corresponding 3D case). In this contribution we follow the idea to virtually create a plane-wave illumination by solving a field synthesis problem with respect to the positions of the transmitting (Tx) antennas, which are located in the NF of the scatterer [12], [13]. A related procedure was recently reported for rectangular planar scan apertures in [14] to determine the location of point scatterers, from which the RCS was then computed. Our approach, however, aims at reconstructing the 3D monostatic RCS without any linearizing assumptions from a set of limited bistatic NF scattering data, where the measurement samples may be distributed almost arbitrarily around the Tx antenna. For every Tx position, an inverse source problem is solved for the excitation dependent plane-wave spectrum of the equivalent sources. The results are combined using the antenna weights, found by solving the field synthesis problem with respect to the Tx positions. Moving the Tx and receiving (Rx) antennas around the object under test (or similarly by rotating the object), the full 3D RCS may be reconstructed. Both, the incident as well as the scattered field, are expanded in propagating plane waves on the unit sphere, which allows an efficient implementation for all kinds of scan geometries [15], [16]. Consequently, as strong irregularities of the (known) measurement sample locations do not pose a problem, one may even envision a setup where a number of unmanned aerial vehicles (UAVs) carry the probe antennas and scan the scattered field around the transmitter.

II. Theory

A. Inverse Source Problem

We consider a scattering problem as shown in Fig. 1. The Tx antenna m creates the incident field $\boldsymbol{E}_{\mathrm{inc}}$ illuminating the scattering object. The resulting scattered field $\boldsymbol{E}_{\mathrm{sca}}(\boldsymbol{r})$ may be expressed in terms of excitation dependent equivalent electric and magnetic current densities $\boldsymbol{J}_{\mathrm{eq}}(\boldsymbol{r}', \boldsymbol{\nu}_m)$ and $\boldsymbol{M}_{\mathrm{eq}}(\boldsymbol{r}', \boldsymbol{\nu}_m)$ as

$$\boldsymbol{E}_{\mathrm{sca}}(\boldsymbol{r}, \boldsymbol{\nu}_m) = \iint_{V_s} \left[\overline{\mathbf{G}}_J^E(\boldsymbol{r}, \boldsymbol{r}') \cdot \boldsymbol{J}_{\mathrm{eq}}(\boldsymbol{r}', \boldsymbol{\nu}_m) + \overline{\mathbf{G}}_M^E(\boldsymbol{r}, \boldsymbol{r}') \cdot \boldsymbol{M}_{\mathrm{eq}}(\boldsymbol{r}', \boldsymbol{\nu}_m) \right] \mathrm{d}v', \quad (1)$$

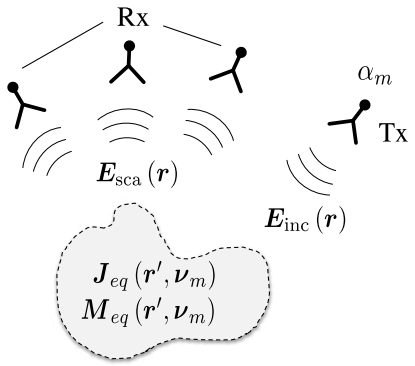

Fig. 1. Scattering problem with single transmitting antenna m and equivalent electric and magnetic current densities $\boldsymbol{J}_{\mathrm{eq}}$, and $\boldsymbol{M}_{\mathrm{eq}}$, creating the scattered field $\boldsymbol{E}_{\mathrm{sca}}$.

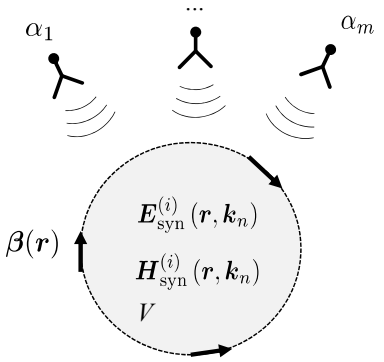

Fig. 2. Synthesizing the electric field of a plane wave with wave vector $\boldsymbol{k}$ and polarization (i) within the volume V. The tangential fields are tested on the discretized surface of V by RWG basis functions $\boldsymbol{\beta}(\boldsymbol{r})$.

where $\overline{\mathbf{G}}_J^E$ and $\overline{\mathbf{G}}_M^E$ are the free space dyadic Green's function of the electric field for electric and magnetic currents, respectively. The parameter $\boldsymbol{\nu}_m$ indicates here the dependency on the Tx antenna m. Employing an expansion in propagating plane waves on the unit sphere, (1) may as well be written as [16]

$$\boldsymbol{E}_{\mathrm{sca}}(\boldsymbol{r}, \boldsymbol{\nu}_m) \approx \oiint \tilde{\boldsymbol{Q}}(\boldsymbol{k}, \boldsymbol{\nu}_m)\, T_L\left(\hat{k} \cdot \hat{D}, kD\right) \mathrm{d}^2\hat{k}, \quad (2)$$

where T_L is the fast multipole method (FMM) translation operator of order L and for a translation vector $\boldsymbol{D} = \boldsymbol{r} - \boldsymbol{r}_Q$, with $\boldsymbol{r}_Q$ being the reference point of the expansion. $\tilde{\boldsymbol{Q}}(\boldsymbol{k}, \boldsymbol{\nu}_m)$ is the (also excitation dependent) plane-wave spectrum of the equivalent current densities. By measuring the scattered field on an arbitrarily shaped scan surface around the transmitting antenna, one can setup a linear system of equations to solve for the scattered plane-wave spectrum. The size of the scan surface determines the valid angular range in $\boldsymbol{k}$-space, where we obtain a correct solution of $\tilde{\boldsymbol{Q}}(\boldsymbol{k}, \boldsymbol{\nu}_m)$. As will be shown, this becomes particularly important for constructing the monostatic RCS solution. The linear system of equations is efficiently solved by employing hierarchical grouping as described in [15] and a GMRES solver, yielding the least mean square solution [17].

B. Plane-Wave Synthesis

As depicted in Fig. 2, the electric field of an incident plane wave with polarization (i) and wave vector $\boldsymbol{k}_n$ may be synthesized in a target volume V by choosing M antenna input weights α according to [13]

$$\boldsymbol{E}^{(i)}_{\mathrm{syn}}(\boldsymbol{r}, \boldsymbol{k}_n) \approx \oiint \sum_{m=1}^{M} \alpha_m^{(i)}(\boldsymbol{k}_n)\, \tilde{\boldsymbol{W}}_m(\boldsymbol{k}) \, T_L\left(\hat{k} \cdot \hat{D}_m, kD_m\right) \mathrm{d}^2\hat{k}, \quad (3)$$

where $\tilde{\boldsymbol{W}}_m(\boldsymbol{k})$ is the plane-wave spectrum of the transmitting antenna m and T_L is again the FMM translation operator of order L. To setup a linear system of equations, the target volume is enclosed by a triangular surface mesh, on which the synthesized field is tested by means of RWG functions $\boldsymbol{\beta}(\boldsymbol{r})$. Again, a GMRES solver is employed to obtain the antenna weights α_m.

C. Monostatic RCS Computation

With the known antenna weights $\alpha_m^{(i)}(\boldsymbol{k}_n)$ for two polarizations (i) and having determined the scattered plane-wave spectra $\tilde{\boldsymbol{Q}}_m^{(i)}(\boldsymbol{k}, \boldsymbol{\nu}_m)$ for all corresponding Tx antenna positions m, the dyadic bistatic scattering spectrum

$$\overline{\mathbf{Q}}(\boldsymbol{k}, \boldsymbol{k}_n) = \begin{bmatrix} Q_{\mathrm{VV}}(\boldsymbol{k}, \boldsymbol{k}_n) & Q_{\mathrm{VH}}(\boldsymbol{k}, \boldsymbol{k}_n) \\ Q_{\mathrm{HV}}(\boldsymbol{k}, \boldsymbol{k}_n) & Q_{\mathrm{HH}}(\boldsymbol{k}, \boldsymbol{k}_n) \end{bmatrix}$$

can be computed. Due to the truncation of the scan surface when measuring the scattered field, $\tilde{\boldsymbol{Q}}_m^{(i)}(\boldsymbol{k}, \boldsymbol{\nu}_m)$ is only valid in a limited angular region around the transmitter m. However, as we are only interested in determining the *monostatic* scattering spectrum $\overline{\mathbf{Q}}(\boldsymbol{k}_n, \boldsymbol{k}_n)$, we only have to make sure that the correct solution at $\boldsymbol{k}_n$ is available for all m. With the known scattering spectrum, the monostatic RCS for an incident plane wave with polarization $\hat{u}_n^{(i)}$ can be directly evaluated as

$$\sigma^{(i)}(\boldsymbol{k}_n, \boldsymbol{k}_n) = 4\pi \| \overline{\mathbf{Q}}(\boldsymbol{k}_n, \boldsymbol{k}_n) \cdot \hat{u}_n^{(i)} \|^2. \quad (4)$$

III. Numerical Results

To test the field synthesis approach we aim at creating the field of a linearly polarized plane wave within a spherical target volume with radius $r_V = 0.5\,\mathrm{m}$. The plane wave is incident from the positive x-direction at $\vartheta = 90°$. The transmitting antennas are distributed along a spherical grid with $r_{\mathrm{meas}} = 2.5\,\mathrm{m}$ and $\Delta\varphi = \Delta\vartheta = 5°$ around the direction of incidence, with a maximum angular range of $\pm 15°$, which results in 58 Tx antenna positions. The frequency was set to 1 GHz for this example and we work with Hertzian dipoles. The relative error of the synthesized field with respect to the ideal plane-wave field $\boldsymbol{E}_{\mathrm{pw}}$,

$$\mathcal{E}(\boldsymbol{r}) = \frac{\| \boldsymbol{E}_{\mathrm{syn}}(\boldsymbol{r}) - \boldsymbol{E}_{\mathrm{pw}}(\boldsymbol{r}) \|}{\max \| \boldsymbol{E}_{\mathrm{pw}} \|}, \quad (5)$$

is shown in Fig. 3 and is obviously around $-50\,\mathrm{dB}$ within the target volume.

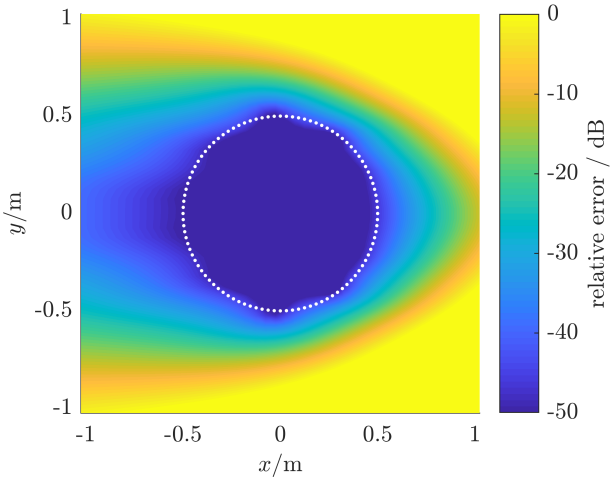

Fig. 3. Relative error of the synthesized electric field of a plane wave, incident from $\vartheta = 90°$, $\varphi = 0°$, using transmitters on a spherical grid with radius $r_{\text{meas}} = 2.5\,\text{m}$ and maximum angular range of $\pm 15°$ around the direction of incidence. The target volume was a sphere with radius $r_V = 0.5\,\text{m}$, indicated by the dotted line.

The same field synthesis setup is now used to determine the monostatic RCS of the perfectly electrically conducting (PEC) test object shown in Fig. 4. The object is composed of an open cuboid, having an edge length of around $0.45\,\text{m}$ and has some open and closed cylinders, as well as a dihedral corner reflector attached to it. The geometry was chosen such that strong multiple interactions at the object can be expected. As indicated in Fig. 4, the Tx antenna is still moved on a spherical grid with $r_{\text{meas}} = 2.5\,\text{m}$ and at each position the Rx antennas are irregularly distributed around it. In fact, the locations of the Rx samples follow here a spiral path around the Tx antenna with a maximum radius of $r_{\text{spiral}} = 1.5\,\text{m}$, but with an additional random position offset of $\pm 0.2\,\text{m}$ in

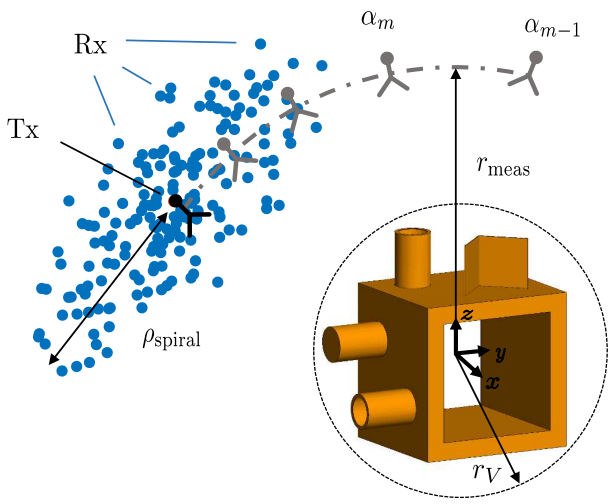

Fig. 4. NF measurement setup for the cubic test object. The NF sample locations are irregularly distributed around the Tx antenna, which is moved on a spherical grid.

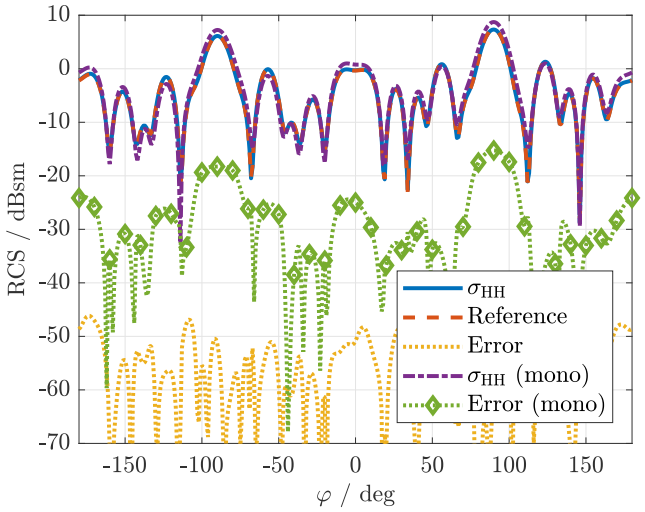

Fig. 5. HH component of the computed monostatic RCS of the cubic test object at $\vartheta = 90°$ using a set of limited bistatic NF scattering data or using an algorithm working on monostatic NF data only ("mono").

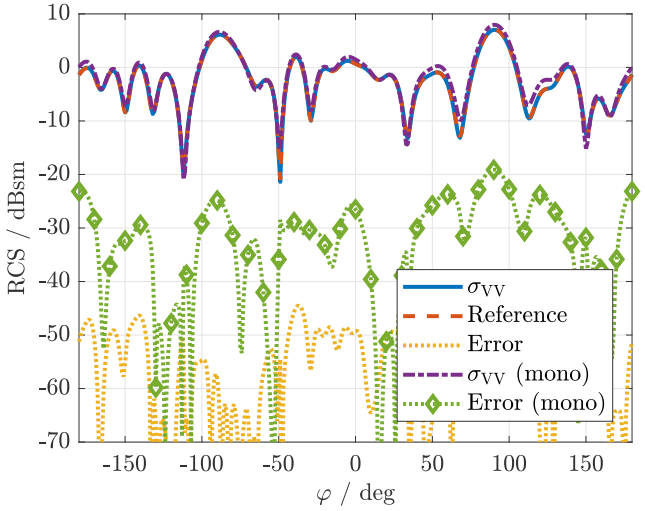

Fig. 6. VV component of the computed monostatic RCS of the cubic test object at $\vartheta = 90°$ using a set of limited bistatic NF scattering data or using an algorithm working on monostatic NF data only ("mono").

x, y and z. This corresponds to 179 NF samples per Tx position, where always two orthogonal field components are acquired. The scattered NF as well as RCS reference data was simulated using the FEKO simulation software [18]. Again, Hertzian dipole probes were used to minimize the simulation effort. Solving all inverse source problems of this setup and using the antenna weights determined from the solution of the field synthesis problem, the monostatic RCS is computed. The mean time for solving one of the inverse source problems was $1.1\,\text{s}$ using 4 threads on an Intel Xeon E5-1630 CPU. Fig. 5 and 6 show the result in a spherical cut at $\vartheta = 90°$ for the HH and VV component, respectively. Additionally, we include a solution using only monostatic NF data on the spherical grid of the Tx antenna and employing the linearized algorithm described in [9]. With the presented approach, the

TABLE I
MAXIMUM ERRORS OF THE COMPUTED MONOSTATIC RCS OF THE CUBIC TEST OBJECT USING A LIMITED SET OF BISTATIC NF SCATTERING DATA.

Cut	VV	HV	VH	HH
$\varphi = 0°$	$-43.9\,\mathrm{dB}$	$-55.1\,\mathrm{dB}$	$-50.5\,\mathrm{dB}$	$-45.1\,\mathrm{dB}$
$\varphi = 90°$	$-42.0\,\mathrm{dB}$	$-53.4\,\mathrm{dB}$	$-46.9\,\mathrm{dB}$	$-44.7\,\mathrm{dB}$
$\vartheta = 90°$	$-44.5\,\mathrm{dB}$	$-49.9\,\mathrm{dB}$	$-56.3\,\mathrm{dB}$	$-46.2\,\mathrm{dB}$

relative magnitude error with respect to the reference solution is obviously as low as $-45\,\mathrm{dB}$ and mainly limited by the accuracy of the field synthesis, whereas it reaches $-15\,\mathrm{dB}$ for the linearized method. In Table I the maximum relative errors of all components in the principle cut planes are summarized.

In order to experimentally validate the algorithm, NF scattering measurements were performed in the anechoic measurement chamber of the Technical University of Munich (TUM). While a spherical positioner is used to rotate the target object, the transmitting open ended waveguide (OEWG) probe is moved on a planar grid around the receiving (dual polarized) horn antenna as shown in Fig. 7. The covered scan area has a size of $2.4\,\mathrm{m} \times 1.6\,\mathrm{m}$, not including, however, the area directly below the Rx antenna, which is mounted on a static mast. All four orthogonal scattering components are measured by rotating the Tx antenna by $90°$ at each Tx position. Additionally, an empty chamber measurement was acquired to subtract the incident field from the measurement samples. The measurements were performed at a frequency of $4\,\mathrm{GHz}$. The target is a physical model of the cubic test object that was already used for the simulations and is shown in Fig. 8. Rotating the object with $2°$ angular step width in ϑ

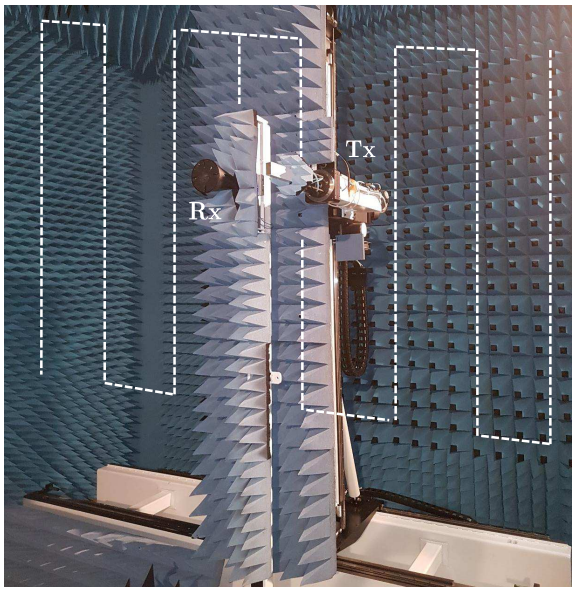

Fig. 7. Setup for bistatic NF scattering measurements. The transmitting OEWG antenna (Tx) is moved along the dashed scan path around the static receiving horn antenna (Rx).

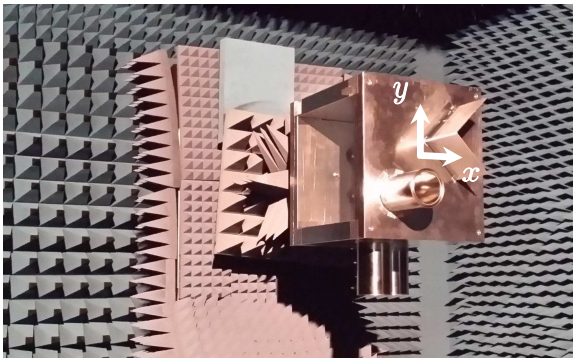

Fig. 8. Cubic test object at the spherical positioner in the anechoic chamber of TUM.

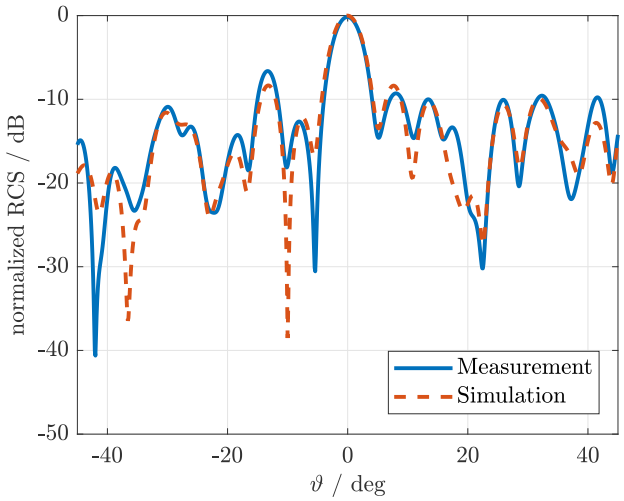

Fig. 9. Normalized HH component of the monostatic RCS of the cubic test object, determined from measured NF data, compared to FEKO simulation data at $\varphi = 0°$.

and φ, the complete upper hemisphere was scanned for 144 positions of the Tx antenna, corresponding to a $\lambda/2$ sampling of the planar scan area with respect to the minimum sphere of the test object. Due to the size of the planar scan area and a measurement radius of the Rx probe $r_{\mathrm{meas}} = 2.65\,\mathrm{m}$, the maximum angular range for synthesizing the plane wave was limited to $\pm 16°$. Still, within the spherical target volume enclosing the test object, a mean error of the synthesized field of about $-45\,\mathrm{dB}$ is theoretically possible. Again, all inverse source problems are solved and the monostatic RCS is computed. In this case, the mean time for solving one of the inverse source problems was about $1.6\,\mathrm{s}$. The result is shown in Fig. 5 for a spherical cut at $\varphi = 0°$, depicting the normalized RCS for the HH component. As a reference, the simulated RCS of the PEC FEKO model for this frequency is included. Obviously, the qualitative agreement is quite good, considering the fact that the simulation model cannot perfectly represent the real test object and that our setup will inevitably be subject to some measurement errors, such as parasitic reflections, small misalignments and noise.

IV. Conclusion

By solving a field synthesis problem with respect to the transmitter positions, an incident plane wave can be virtually synthesized to determine the monostatic RCS from a set of bistatic NF measurements. It was demonstrated that the scattered field has to be acquired only in a small angular range around the transmitter, thus reducing the required number of samples significantly compared to a full bistatic setup. Moreover, highly irregular sample distributions are possible, enabling a wide range of measurement scenarios. Compared to a linearized (image based) method, the presented approach does not suffer from inaccuracies in the case of strong multiple interactions at the object, as demonstrated by using simulated and measured NF scattering data.

References

[1] E. Knott, *Radar Cross Section Measurements*. Raleigh, NC, USA: SciTech Pub., 2006.

[2] C. Parini, S. F. Gregson, J. McCormick, and D. J. V. Rensburg, *Theory and practice of modern antenna range measurements*. London, UK: The Institution of Engineering and Technology, 2014.

[3] J. O. Melin, "Measuring radar cross section at short distance," *IEEE Trans. Antennas Propag.*, vol. 35, no. 8, pp. 991–996, Aug. 1987.

[4] B. J. Cown and C. E. Ryan, "Near-field scattering measurements for determining complex target RCS," *IEEE Trans. Antennas Propag.*, vol. 37, no. 5, pp. 576–585, May 1989.

[5] I. J. LaHaie, "Overview of an image-based technique for predicting far-field radar cross section from near-field measurements," *IEEE Antennas Propag. Mag.*, vol. 45, no. 6, pp. 159–169, Dec 2003.

[6] M. A. Dinallo, "Extension of plane-wave scattering-matrix theory of antenna - antenna interactions to three antennas: A near-field radar cross section concept," in *Proc. Antenna Applications Symposium*, vol. 2, Urbana, IL, USA, Sep. 1984, pp. 665–686.

[7] D. G. Falconer, "Extrapolation of near-field RCS measurements to the far zone," *IEEE Trans. Antennas Propag.*, vol. 36, no. 6, pp. 822–829, Jun 1988.

[8] T. Vaupel and T. F. Eibert, "Comparison and application of near-field ISAR imaging techniques for far-field radar cross section determination," *IEEE Trans. Antennas Propag.*, vol. 54, no. 1, pp. 144–151, Jan. 2006.

[9] G. Schnattinger, R. A. M. Mauermayer, and T. F. Eibert, "Monostatic radar cross section near-field far-field transformations by multilevel plane-wave decomposition," *IEEE Trans. Antennas Propag.*, vol. 62, no. 8, pp. 4259–4268, Aug. 2014.

[10] O. Neitz and T. F. Eibert, "Fourier based 3D ISAR near-field imaging and radar cross section transformation," in *Proc. International Conference on Electromagnetics in Advanced Applications (ICEAA)*, Torino, Italy, Sep. 2015, pp. 1198–1201.

[11] O. M. Bucci and M. D. Migliore, "Effective estimation of 2-D monostatic radar cross sections from near-field measurements," *IEEE Trans. Antennas Propag.*, vol. 54, no. 2, pp. 750–752, Feb. 2006.

[12] O. M. Bucci, M. D. Migliore, G. Panariello, and D. Pinchera, "Plane-wave generators: Design guidelines, achievable performances and effective synthesis," *IEEE Trans. Antennas Propag.*, vol. 61, no. 4, pp. 2005–2018, April 2013.

[13] R. A. M. Mauermayer, Y. Weitsch, and T. F. Eibert, "Electromagnetic field synthesis by hierarchical plane wave-based field transformation," *IEEE Trans. Antennas Propag.*, vol. 63, no. 12, pp. 5561–5572, Dec. 2015.

[14] K. L. Ford, J. C. Bennett, and D. G. Holtby, "Use of a plane-wave synthesis technique to obtain target RCS from near-field measurements, with selective feature extraction capability," *IEEE Trans. Antennas Propag.*, vol. 61, no. 4, pp. 2051–2057, Apr. 2013.

[15] T. F. Eibert, E. Kilic, C. Lopez, R. A. M. Mauermayer, O. Neitz, and G. Schnattinger, "Electromagnetic field transformations for measurements and simulations (invited paper)," *Progress in Electromagnetics Research*, vol. 151, pp. 127–150, 2015.

[16] O. Neitz, R. A. M. Mauermayer, Y. Weitsch, and T. F. Eibert, "A propagating plane-wave-based near-field transmission equation for antenna gain determination from irregular measurement samples," *IEEE Trans. Antennas Propag.*, vol. 65, no. 8, pp. 4230–4238, Aug 2017.

[17] Y. Saad, *Iterative Methods for Sparse Linear Systems*, 2nd ed. Society for Industrial and Applied Mathematics, 2003.

[18] Altair Engineering, Inc., FEKO. [Online]. Available: http://feko.info